A STUDY OF ULTRASONIC LIVER IMAGES CLASSIFICATION WITH ARTIFICIAL NEURAL NETWORKS BASED ON FRACTAL GEOMETRY AND MULTIRESOLUTION ANALYSIS

WEN-LI LEE[1], KAI-SHENG HSIEH[2], YUNG-CHANG CHEN[3], YING-CHENG CHEN[3]

[1]Department of Information Management, Kang Ning Junior College of Medical Care and Management, Taipei, Taiwan
[2]Department of Pediatrics, Veterans General Hospital, Kaohsiung, Taiwan
[3]Department of Electrical Engineering, National Tsing Hua University, Hsinchu, Taiwan

ABSTRACT

In this study, we evaluate the accuracy of classifiers for classification of ultrasonic liver tissues. Two different statistic classifiers and three various artificial neural networks are included: Bayes classifier, k-nearest neighbor classifier, Back-propagation neural networks, probabilistic neural network and modified probabilistic neural network. These five different classifiers were investigated to determine their ability to classify various categories of ultrasonic liver images. The investigation was performed on the basis of the same feature vector. For statistic classifiers the classification accuracy is at most 90.7% and with artificial neural networks the accuracy is at least 92%. The experimental results illustrated that artificial neural networks are an attractive alternative to conventional statistic techniques when dealing with classification task. Moreover, the feature vector based on fractal geometry and wavelet transform can provide good discriminant ability for ultrasonic liver images under study.

Biomed Eng Appl Basis Comm, 2004(April); 16: 59-67.
Keywords: Classification, artificial neural networks, fractal geometry, wavelet transform, multiresolution analysis, statistic classifiers.

1. INTRODUCTION

Ultrasound imaging is widely used technique in the diagnosis of soft tissues, due to its ability to visualize human tissue without deleterious effects. Meanwhile, it enables the operator to quickly locate the desired image plane to exhibit normal or pathological anatomy precisely. It is also economical in medical expenditure.

Currently, the clinical diagnosis is based on visual interpretation of images by specialized physicians. One application of diagnostic ultrasound is liver imaging, from which the most useful tissue differentiation techniques can be obtained based on the investigation of B-scan images [1-10]. Via visual interpretation of B-scan images, a clinician can diagnose the tissue by observing the brightness and texture compared to surrounding areas [11]. Hence, liver tissue characterization using ultrasound apparatus mainly depends on the ability of the clinician to observe certain textural characteristics. However, a visual

Received: Dec 8, 2003; Accepted: Dec 25, 2003
Correspondence: Kai-Sheng Hsieh, M.D.
Department of Pediatrics, Veterans General Hospital, Kaohsiung, Taiwan
E-mail: kshsieh@isca.vghks.gov.tw

criterion of diagnosing liver diseases principally depends on the clinical experience of physicians and it is extremely subjective. Hence, there have been many endeavors to develop objective tissue characterization criteria on the premise that there is much more observer-independent information obtainable from ultrasound than what is currently being used. These are rooted on the primary notion that the biological tissue are composed of characteristic structures whose ultrasonic properties often change due to diseases. The object of tissue characterization is the extraction of signatures that assume diverse values in the present of normal and diseased states of tissues, such that it is possible to discriminate between them.

Since ultrasound B-scan images present various granular structures as texture, the analysis of ultrasound image is similar to the problem in texture analysis. The most important aspect for texture analysis is to define a set of meaningful features. A considerable number of texture analysis techniques were developed over the years. The most common are the spatial gray-level dependence matrices [12], the Fourier power spectrum [13], the gray-level difference statistics [14], Laws' texture energy measures [15], and filtering approaches [16-25]. Although they yield promising results to general texture analysis, they are unable to classify ultrasonic liver images adequately but fractal analysis [16-17], [22-25]. Lee *et al.* [22-25] have proposed a texture feature based upon wavelet transform and fractal geometry to detect liver diseases quickly and accurately.

Fractal geometry as initially developed by Mandelbrot [26] has had a major impact in modeling and analysis in natural and physical sciences. Fractal provides a suitable mathematical framework to investigate uneven and complex shapes that exist in nature. Hence, if the pixel intensity of ultrasound B-scan images is regarded as the height above a plane then the intensity surface can be viewed as a coarse surface. A fundamental feature of fractal geometry is that it enables the characterization of irregularity that may not be treated generally in Euclidean geometry. Therefore, among fractal features, fractal dimension is one of the most essential features. Texture features based on fractal dimensions have been applied successfully to texture classification [16-17], [22-25], [27-28]. Generally, single fractal dimension is not sufficient to discriminate among most real-world textures since its dynamic range for an image is limited between two and three only. Wu *et al.* [16-17] and Lee *et al.* [22-25] have proposed a fractal feature vector based on multiple resolutions imagery or multi-threshold concepts. Alternately, it has been established previously that the fractal feature vector, based on standard pyramid wavelet transform and fractal geometry, is a proper feature-extraction method for texture classification [22-25].

Another important issue in texture analysis is the choice of an appropriate classifier. There are basically two types of classifiers; statistic classifiers which include: linear discriminant, maximum likelihood and k-nearest neighbor classifiers, and the artificial neural-network classifiers which include: multilayer backpropagation neural network (BPNN), probability neural network (PNN) and Learning Vector Quantization (LVQ), etc. Owing to the fact that the characteristics of ultrasonic liver images are highly complex and difficult to classify, artificial neural network classifiers through their adaptive learning nature offer attractive and computationally very efficient alternatives.

In this study, the artificial neural-network-based classification schemes based on fractal geometry and wavelet transform for ultrasonic liver images are discussed. This paper is organized as follows: Feature extraction scheme is presented in the following section. Section III clarifies the pattern classification techniques. The experimental results and discussions are given in Section IV respectively. Finally, conclusions follow.

2. FEATURE EXTRACTION SCHEME

Feature extraction is a crucial step for any pattern recognition task especially for ultrasonic liver tissues classification since liver images are highly complex and it is difficult to define a reliable and robust feature vector. Generally, ultrasound B-scan images present various granular structures as texture; the analysis of ultrasound image is analogous to the problem in texture analysis. However, textural features are those characteristics such as smoothness, fineness and coarseness or certain pattern associated with an image [12]. They reflect the local spatial distribution property in a certain region. Lee et al. [22-25] have proposed a fractal feature vector based on multiple resolutions imagery. The scheme can extract features which contain contributions from both the spectral and textural aspects. In the following, the feature extraction scheme is briefly reviewed.

2.1 Estimation of Fractal Dimension

Mandelbrot [26] defines fractal as a bounded set for which the Hausdorff Besicovitch dimension strictly exceeds the topological dimension, where Hausdorff Besicovitch dimension or fractal dimension is a real number used to describe the shape and appearance of objects that have the property of self-similarity. The property of self-similarity or scaling, as exemplified by

coastline, Von Koch curve, and the Mandelbrot set, is one of the fundamental concepts of fractal geometry. The concept of self-similarity can be best employed to estimate the fractal dimension.

Consider a bounded set A in Euclidean n-space. The set A is said to be self-similar when A is the union of N_r non-overlapping copies of itself, each of which has been scaled down by a ratio r in all coordinates. The fractal dimension D_f of A can be obtained from the relation [26],

$$D_f = \lim_{r \to 0} \frac{\log(N_r)}{\log(1/r)} \tag{1}$$

While the definition of fractal dimension by self-similarity is straightforward, it can scarcely be calculated from the image data. However, a related measure of fractal dimension can be computed from a fractal set, A, in $\Re^n$. Several approaches exist to calculate fractal dimension in an image. The most popular measure is box counting [29-33]. Among the varieties of box-counting approaches, the Differential Box Counting (DBC) method [29] that has a large dynamic range and computational efficiency is adopted herein. Hence, is calculated as follows [24-25], [29-30]:

If an image of $M \times M$ pixels has been scaled down to $L \times L$ pixels where $1 < L \leqq M/2$ and L is an integer. Thus the scale ratio r is L/M. The image can be viewed as a three-dimensional (3D) space with (x, y) indicates the two-dimensional (2D) position and the third coordinate (z) denoting gray-level. The (x, y) space is partitioned into grids of size $L \times L$. On each grid, there is a column of boxes of size $L \times L \times L'$. If the total number of gray-levels is G, then $L' = [L \times G/M]$. Let the minimum and the maximum gray-level of the image in the (i, j)th grid both fall in the box number k and l, as illustrated in Fig.1. Then

$$n_r(i, j) = l - k + 1 \tag{2}$$

is the contribution of N_r in the (i, j)th grid. Taking contributions from all grids, the following is produced:

$$N_r = \sum_{i,j} n_r(i, j) \tag{3}$$

where N_r is counted for differing values of r (*i.e.* differing values of L). Then using(1), the fractal dimension D_f can be estimated from the least-squares linear fitting of $\log(N_r)$ versus $\log(1/r)$.

2.2 General Multiresolution Analysis Based on M-band Wavelet Transforms

By multiresolution analysis, a signal can be decomposed into numerous details at various resolutions where each resolution represents various physical structures in the signal. This coincides with processing visual information in the early stages of the human visual system. Campbell et al. [34] first proposed the theory to support that the visual system decomposes the retinal image into a number of filtered images. Each filtered image contains intensity variations over a narrow range of frequency and orientation. The psychophysical experiments that suggested such decomposition used various grating patterns as stimuli and were based on adaptation techniques. Subsequent psychophysiological experiments provided additional evidence upholding the theory [35]. Therefore, the theory gives an impetus to describe a signal by decomposing it into subbands, and each subband can then be treated alone, based on its feature. Mallat [36] has illustrated that this multiresolution representation of an image can be interpreted as its decomposition by a wavelet basis set. Multiresolution analysis in the 2-band case is referenced in [36-45]:

Using M-band wavelets [38], [40], [42-45], the general multiresolution analysis provides a more flexible tiling of the time-scale plane than that resulting from the two-band multiresolution analysis, which is important for the analysis of middle-frequency or high-frequency signals as it reveals useful features from the subbands.

Given a one-dimensional signal, the full discrete wavelet expansion can be represented as

$$f(t) = \sum_{k=-\infty}^{\infty} c_J(k) M^{J/2} \phi(M^J t - k) + \sum_{j=J}^{\infty} \sum_{\ell=1}^{M-1} \sum_{k=-\infty}^{\infty} d_{\ell,j}(k) M^{j/2} \psi_\ell(M^j t - k), \tag{4}$$

where the expansion coefficients are determined by

$$c_J(k) = \left\langle f(t), M^{J/2} \phi(M^J t - k) \right\rangle = \int f^*(t) M^{J/2} \phi(M^J t - k) dt \tag{5}$$

and

$$d_{\ell,J}(k) = \left\langle f(t), M^{J/2} \psi_\ell(M^J t - k) \right\rangle = \int f^*(t) M^{J/2} \psi_\ell(M^J t - k) dt, \tag{6}$$

where $\phi(t)$ is called scaling function that satisfies the dilation equation:,

$$\phi(t) = \sqrt{M} \sum_k h_0(k) \phi(Mt - k), \tag{7}$$

with $h_0(k)$ denoting scaling filter and satisfying certain constraints [40], [42], [44]. $\psi_\ell(t)$, ℓ=1,2,... ,M-1, are called wavelet functions that satisfy the wavelet equations:

$$\psi_\ell(t) = \sqrt{M}\sum_k h_\ell(k)\phi(Mt-k) \quad \text{for } \ell = 1,2,\cdots,M-1, \tag{8}$$

with $h_\ell(k)$ denoting the ℓ-th wavelet filter and satisfying certain constraints [38], [40-41]. $\{\phi(t), \psi_\ell(t), \ell=1,2, ..., M-1\}$ are mutually orthogonal functions.

The filters $h_0(k)$ and $h_\ell(k)$, ℓ=1,2,... ,M-1, play a essential role in a given wavelet transform. To achieve M-band discrete wavelet transform, the explicit forms of $\phi(t)$ and $\psi_\ell(t)$ are not required but only depend on $h_0(k)$ and $h_\ell(k)$, which must meet several conditions [36-45]. Hence, an M-band wavelet basis can be completely specified by the choice of the scaling filter (*i.e.* $h_0(k)$) and M-1 wavelet filters (i.e. $h_\ell(k)$, ℓ=1,2,... ,M-1). A typical M-channel filter bank based on Mallat's fast algorithm [38] is shown in Fig. 2. That is, the filter bank furnishes an easy way to relate the coefficients of M-band wavelet analysis at different levels of decomposition.

The above wavelet model can be generalized to any dimension. There are diverse extensions of one-dimensional wavelet transform to two dimensions. The easiest way to extend one-dimensional wavelet transform to two dimensions is the introduction of separable 2-D scaling and wavelet functions as the tensor products of their one-dimensional wavelet basis functions along the horizontal and vertical directions.

2.3 The Multiresolution Fractal Feature Vector Based on *M*-band Wavelet Transform

An important aspect of texture analysis is to develop a set of texture measures that can successfully discriminate textures. The feature extraction scheme by traditional multiresolution analysis based on standard wavelet transform decomposes subimages recursively in the low frequency channel. Since the most significant information of a texture often appears in the middle frequency channels rather than the low frequency ones. Further decomposition in only the lower frequency channels may not provide satisfactory discriminative information to texture analysis [18].

The *M*-band wavelet transform is an outstanding means to portray signals at various scales, and decomposes a signal by projecting it onto a family of functions that are generated from a wavelet basis through its dilations and translations. Thus, an image is transformed into M^2 resolution cells. This filtering can obtain the desired regularizations inherently.

General multiresolution analysis based on wavelet transform provides more significant features [23], [25]. Hence, the fractal feature vector based on general multiresolution analysis has been defined as [23], [25]

$$MF \equiv (D_f^{m,i}, D_f^{m,i+1}, \cdots, D_f^{m-n+1,i}, \cdots, D_f^{m-n+1,i+k}), \tag{9}$$

where $D_f^{m,i}$ denotes the fractal dimension of the *i-th* subimage at scale level *m*.

3. PATTERN CLASSIFICATION TECHNIQUE

In the following subsection, the classification techniques that adopted in this study are reviewed, which give us the foundation for performance comparisons.

A. Statistical Classifiers

1) Bayes Classifier [46-48]: The Bayes classifier is applied to investigate the feasibility of classifying texture image, since from the statistical viewpoint, it represents the optimum measure of performance. The Bayesian decision rule classifies an observation to the class that has the highest a posteriori probability among the classes. One of the ways to represent a pattern classifier is in terms of a set of discriminant functions $g_i(X)$, i=1,$\cdots$, K where K is the total number of classes. The classifier is to assign a feature vector X to class ω_i if $g_i(X) > g_j(X)$ for all $j \neq i$. Let us assume that the distribution of feature vectors X within the ith class $P(X|\omega_i)$ is a multivariate normal distribution with mean vector μ_i and covariance matrix C_i and the *a priori* probabilities are equal for all classes. Under such an assumption, the discriminant functions can be defined as

$$g_i(X) = -\frac{1}{2}(X-\mu_i)^T C_i^{-1}(X-\mu_i) - \frac{1}{2}\log|C_i| + \log P(\omega_i). \tag{10}$$

2) *k*-Nearest Neighbor (*k*-NN) Classifier [47-48]: In a *k*-NN classifier, each class is represented by a set of prototype vectors. The k closest neighbors of a pattern vector are found from among all the prototypes. Hence, the class label is decided by the majority rule; that is, assuming that the number of voting neighbors is $k = \sum_{i=1}^{M} k_i$ (where k_i is the number of observations from class ω_i in the set of k neighbors), the classification rule is to assign the test sample to the class that has the largest proportion $\frac{k_i}{k}$.

B. Neural Network Classifiers

Neural network classifiers have shown promise in pattern classification and are considered as a potential alternative approach to statistical pattern classification.

1) Back-propagation Neural Network (BPNN) [49]: Back-propagation is currently the most popular method for performing the supervised learning task. In supervised learning, we try to adapt an artificial neural network so that its output comes close to certain target output for a training set. The goal is to adapt the parameters of the network so that it performs well for patterns from outside the training set. In this study, the BPNN uses 2-layer structure, one 15-neutron hidden layer with hyperbolic tangent transfer function and one 3-neutron output layer with linear transfer function, and utilize the Levenberg-Marquardt algorithm as learning rule to speedup the convergence.

2) Probabilistic Neural Network (PNN) [50-51]: The network structure of PNN is similar to back-propagation; the primary difference is that the transfer function is replaced by exponential function and all training samples are stored as weight vectors.

Let X_{ki}, k=1,$\cdots$, L_i be sample patterns belonging to a class ω_i, the estimator of this class is

$$f_i(X) = \frac{1}{L_i}\frac{1}{(2\pi)^{N/2}\sigma^N}\sum_{k=1}^{L_i} \exp[-\frac{(X - X_{ki})^T(X - X_{ki})}{2\sigma^2}] \quad (11)$$

where

k = pattern number,

L_i = total number of training patterns belonging to class ω_i,

X_{ki} = kth training pattern from class ω_i,

σ = smoothing parameter.

The smoothing parameter σ is used to describe the sharpness of each sample pattern distribution; the smoothing parameter σ is 0.1 in this study. The network is trained by setting the weight vectors in one of the pattern units equal to each pattern X_{ki} in the training set, which is the key feature, and then connecting the output of the pattern units to the appropriate summation unit.

3) Modified Probabilistic Neural Network (MPNN) [52-53]: A network with the same function structure of the PNN but with a number of nodes per class in the hidden layer much lower than the number of training patterns can give classification results approximating those of the PNN. The design of neural network becomes one of defining the number of reference vectors and their location in the pattern space. The learning vector quantization (LVQ) technique is adopted in MPNN, for the algorithm is

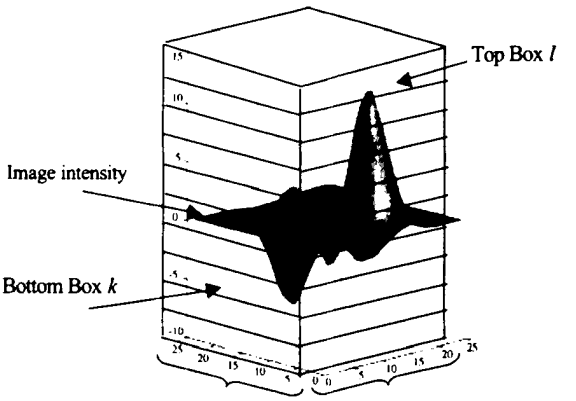

Fig. 1. Determination of n_r.

Fig. 1. Determination of n_r.

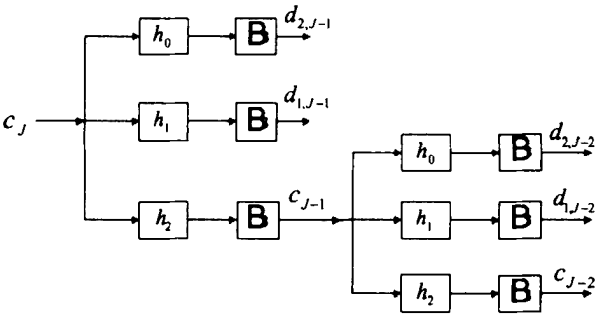

Fig. 2. Filter bank structure for a three-band wavelet system in one dimension.

computationally extremely light and the convergence is reasonably fast. The learning procedure can be described as follows:

(i) Define the total number of reference patterns.

(ii) Assign to each class a number of nodes for hidden layer in proportion to the a priori probability of occurrence of that class.

(iii) Run the LVQ training procedure by using all the available training patterns; the result of this step defines the weight vector relating to the connection from the input to the hidden layer.

(iv) Connect the output of each unit of the hidden layer to the appropriate summation unit of the output layer.

After the training phase has ended, the proposed network performs the same operation of the PNN but with a reduced number of elements in the hidden layer. The smoothing parameter σ is also 0.1 in this case.

4. EXPERIMENTAL RESULTS AND DISCUSSIONS

A. Image Acquisition

In this study, ultrasonic liver images were captured from a phased-array system (Aloka SSD-265, Tokyo, Japan) with a 3.5 MHz transducer and were stored as positive ones. These were then scanned by AGFA's DUOSCAN scanner with 32-pixel/cm and 8-bit/pixel resolution. All images were standardized to the same mean intensity (*i.e.* 128) and were verified by a specialized physician. All patients were biopsied for pathological diagnosis; therefore there is a basis of truth in this study. Three sets of ultrasonic liver images, each of 50 samples, were taken: cirrhosis, hepatoma, and normal. Each sample of 64x64 pixels was chosen to include solely liver parenchyma without major blood vessels, acoustic shadowing, or any type of distortion. Therefore, we uniformly divide whole samples into training set and test set.

The training set is used to train the classifier, while the test set is used to obtain the success rate of the classifier.

B. Feature Extraction and Selection

In general, an M-band wavelet transform can be constructed by two levels of filter bank [38]. The M value can be different at varying levels. The general multiresolution analysis in Chen et al. [22-25] is implemented by the combinative structure of two-channel and three-channel filter bank as shown in Fig. 3. In fact, from signal processing viewpoint, this combinative structure is equal to six-channel filter bank [38]. At the first level, the LL-band is adopted and the other subbands are discarded. However, the other bands may provide additional useful information [23] , [25]. Since the fractal dimension of each chosen subimage should provide valuable information about individual roughness, if the fractal dimension is less than threshold value α, it means that this subimage has very smooth surface. Based on this observation, the fractal dimension of this subimage is too low to be used as a feature. Therefore, the number of features can be reduced. Hence, the order of features is as follows [25]:

$$MF = (D_f^{3,0}, D_f^{2,1}, D_f^{2,2}, D_f^{1,1}, D_f^{1,2}, D_f^{1,3}, D_f^{1,4}, D_f^{1,5}, D_f^{1,6}), \quad (12)$$

where $D_f^{3,0}$ is the fractal dimension of the original image, $D_f^{2,1}$ is the fractal dimension of the oversampled LL-band subimage (*i.e.* no critical decimation and only low-pass filtering along the abscissa and ordinate), $D_f^{2,2}$ is the fractal dimension of the oversampled LH-band subimage (*i.e.* no critical decimation, simply low-pass filtering along the abscissa and high-pass filtering along the ordinate). The final six components in the feature vector are calculated from the oversampled subimage. Herein, two levels with Daubechies 20-tap filter bank for the first level and three-channel orthogonal filter bank [39] for the second level were employed.

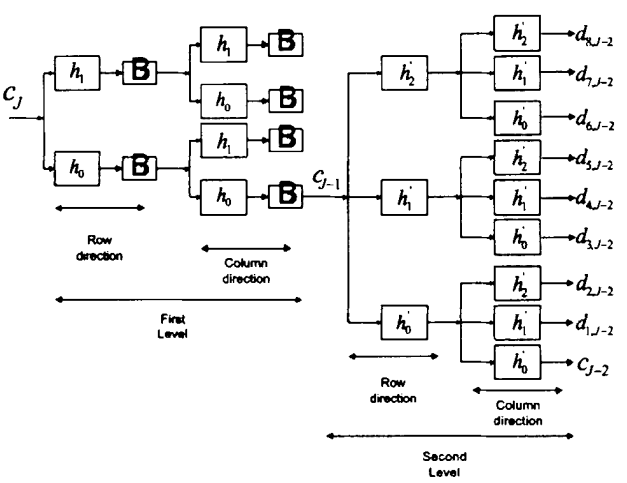

Fig. 3. The general multiresolution analysis: the combinative structure of two-channel and three-channel filter bank.

C. Comparison Study of Various Classifiers

The performances of different kinds of classifiers were examined for their classification accuracy. Table I shows the correct classification rate of test samples for all classifiers considered. The experimental results exhibit that the classifiers using multiresolution fractal feature vector based on wavelet transform is reliable. However, the correct classification rate of k-NN classifier is lower among the five classifiers. Since the performance of the standard k-NN classifier depends on the quality and size of the training set and the performance of the classifier decreases if the available computing resources limit the number of training feature vectors one can use.

The performances of the artificial neural networks considered are better than that of statistic classifiers in this study. The results are expected. In artificial neural networks, the approach has been bottom-up: starting from a very simple linear neuron that computes a weighted sum of its inputs, adding a saturating smooth nonlinearity, and constructing layers of similar parallel units, it turned out that "intelligent" behavior emerged by simple learning rules. Furthermore, the PNN achieved the highest classification rate for classification of ultrasound liver images. However, the key disadvantage of PNN is that if large training sets

Table 1. Liver images classification results for various classifiers

Liver Disease	Correct Classification Rate				
	Bayes	k-NN	BPNN	PNN	MPNN
Normal	92%	92%	96%	92%	92%
Cirrhosis	88%	84%	100%	100%	100%
Hepatoma	92%	88%	88%	96%	84%
Average	90.7%	88%	94.7%	96%	92%

Table 2. Liver images classification results for various classifiers. The training set and test set are reversed with the above test.

Liver Disease	Correct Classification Rate				
	Bayes	k-NN	BPNN	PNN	MPNN
Normal	92%	96%	96%	96%	88%
Cirrhosis	96%	96%	92%	96%	100%
Hepatoma	92%	92%	100%	96%	100%
Average	93.3%	94.7%	96%	96%	96%

are available, the computational cost associated with the testing phase of the PNN is much higher than that of the training phase and can become incompatible with real time classification tasks. Alternatively, the modified probabilistic neural network (MPNN) reduced the computational cost but a gradual degradation of classification performance can be expected as the number of reference vectors in the pattern space is reduced. On the whole, comparing the results obtained using the artificial neural networks with those obtained using conventional discriminant analysis show that the artificial neural networks outperform the statistical classifiers.

From view of pathological anatomy, the trabecular pattern is common and characteristic form of hepatoma. In this form, the tumor cells are arranged in anastomosing plates that are separated by a sinusoidal network. The structure thus resembles that of a normal liver; however the trabeculate is typically wider and less regular [54]. Hence, the hepatoma liver image is rougher than that of a normal liver. The major characteristic of cirrhosis is the hepatic fibrosis that is associated with beginning nodules or fully established nodules [55]. The nodules cause a block structure in the image such that cirrhosis image is rougher than a normal liver image but less rough than hepatoma image. These two liver diseases have rough images of varying degrees. Since ultrasound B-scan liver images demonstrate various granular structures as texture. Generally, texture can be evaluated as being fine, coarse, or smooth. Herein, a fractal feature vector based on M-channel wavelet transform was adopted to determine the most useful information for the characterization of ultrasonic liver images. In the previous works [22-25], the multiresolution fractal feature vector has the best performance among the feature vectors considered. That means that the fractal dimension can provide more useful information for ultrasonic liver image than the other measurements.

The experimental results demonstrated that the fractal model is a good tool to measure the degree of roughness of liver image surfaces. Simultaneously, multiresolution analysis based on wavelet transform indeed provides spectral information of ultrasonic images. To validate the robust of the multiresolution fractal feature vector, we exchange the training set with test set. The result is given in Table II. From the experimental results, the feature vector based on these two analyses can provide a very useful discrimination for ultrasonic liver images.

5. CONCLUSION

In this study, artificial neural networks and statistic classifiers were adopted to classify ultrasonic liver images. Five classifiers are implemented with same type of multiresolution fractal feature vector. From the experimental results, the performance of all classifiers considered is trustworthy and robust. Meanwhile, the multiresolution fractal feature vector provides good discrimination ability to classify the three types of ultrasonic liver images under study. However, in the design of an artificial neural network, two features have to be optimized: convergence and generalization. Future works should include searching for a new powerful and robust feature extraction scheme and a self-adaptation for an artificial neural network.

REFERENCES

1. M. F. Insana, R. F. Wagner, B. S. Garra, D. G. Brown, and T. H. Shawker, "Analysis of Ultrasound image texture via generalized Rician statistics," Opt. Eng., vol. 25, pp. 743-748, 1986.
2. U. Reath, D. Schlaps, and B. Limberg, "Diagnostic accuracy of computerized B-scan texture analysis and conventional ultrasonography in diffuse parenchymal and malignant liver disease," J. Clin. Ultrasound, vol. 13, pp. 87-99, 1985.
3. N. M. Botros, " A microprocessor-based pattern recognition algorithm for in-vivo tissue differentiation," J. Clin. Eng., vol. 13, pp.115-120, 1988.
4. R. Momenan, M. H. Loew, M. F. Insana, R. F. Wagner, and B. S. Garra, "Application of pattern

recognition techniques in ultrasound tissue characterization," 10th Int. Conf. Pattern Recognition, vol. 1, pp. 608-612, 1990.
5. M. F. Insana, R. F. Wagner, B. S. Garra, R. Momenan, and T. H. Shawker, "Pattern recognition methods for optimizing multivariate tissue signatures in diagnostic ultrasound," Ultrasound. Imaging, vol. 8, pp165-180, 1986.
6. B. S. Garra, M. F. Insana, T. H. Shawker, R. F. Wagner, M. Bradford and M. Russell, "Quantitative ultrasonic detection and classification of diffuse liver disease comparison with human observer performance," Invest. Radiology, vol. 24, pp.196-203, 1989.
7. R. F. Wagner, M. F. Insana, and G. Brown, "Unified approach to the detection and classification of speckle texture in diagnostic ultrasound," Opt. Eng., vol. 25, pp. 743-748, 1986.
8. R. Momenan, M. F. Insana, R. F. Wagner, B. S. Garra, and M. H. Loew, "Application of clutter analysis and unsupervised learning to multivariate tissue characterization," J. Clin. Eng., vol. 13, pp.455-461, 1988.
9. R. Momenan, R. F. Wagner, B. S. Garra, M. H. Loew, and M. F. Insana, "Image staining and differential diagnosis of ultrasound scans based on the Mahalanobis distance," IEEE Trans. Medical Imaging, vol. 11, pp. 37-47, June 1994.
10. K. Ogawa, M. Fukushima, K. Kubota, and N. Hisa, "Computer-aided Diagnostic System for Diffuse Liver Diseases with Ultrasonography by Neural Network," IEEE Trans. Nuclear Science, vol. 45, no. 6, pp. 3069-3074, Dec. 1998.
11. G. J. W Simon, E. E. Jane, B. Nigal, E. H. Margaret, E. B. Joe, and W. David, "An ultrasound scoring system for the diagnosis of liver disease in cystic fibrosis," Journal of Hepatology, vol. 22, pp. 513-521, 1995.
12. R. M. Haralick, K. Shanmugam, and I. Dinstein, "Texture features for image classification," IEEE Trans. Systems, Man and Cybernetics, vol. 3, no. 6, pp.610-621, 1973.
13. G. O. Lendaris and G. L. Stanley, "Diffraction pattern sampling for automatic pattern recognition," Proc. IEEE, vol. 58, pp. 198-216, 1970.
14. J. S. Weszka, C. R. Dryer, and A. Rosenfeld, "A comparative study of texture measures for terrain classification," IEEE Trans. Syst., Man, and Cybern., vol. SMC-6, pp. 269-285, 1979.
15. K. I. Laws, Texture image segmentation, Ph.D. dissertation, Image Processing Inst., Univ. of Southern California, 1980.
16. C. M. Wu, Y. C. Chen and K. S. Hsieh, "Texture features for classification of ultrasonic liver images," IEEE Trans. Medical Imaging, vol. 11, pp. 141-152, June 1992.
17. C. M. Wu and Y. C. Chen, "Multi-threshold dimension vector for texture analysis and its application to liver tissue classification," Pattern Recognition, vol. 26, no. 1, pp. 137-144, Jan. 1993
18. T. Chang and C. Kuo, "Texture analysis and classification with tree-structured wavelet transform," IEEE Trans. Image Processing, vol. 2, pp.429-441, Oct. 1993.
19. A. Laine and J. Fan, "Texture classification by wavelet packet signatures," IEEE Trans. Pattern Anal. and Machine Intell., vol. 15, pp. 1186-1191, Nov. 1993.
20. M. Unser, "Texture Classification and segmentation using wavelet frames," IEEE Trans. Image Processing, vol. 4, no. 11, pp. 1549-1560, Nov. 1995.
21. A. Mojsilovi?, M. Popovi?, S. Markovi?, and M. Krsti?, "Characterization of Visually Similar Diffuse Diseases from B-Scan Liver Images Using Nonseparable Wavelet Transform," IEEE Trans. Medical Imaging, vol. 17, no. 4, pp. 541-549, Aug. 1998.
22. Y. C. Chen and W. L. Lee, "Texture Classification Using Multiresolution Fractal Feature Vector," Proc. 4th Asian Conf. On Computer Vision, pp. 204-209, 2000.
23. W. L. Lee, Y. C. Chen and K. S. Hsieh, "Multiresolution fractal feature vector based on M-band wavelet transform," The 2001 IEEE International Symposium on Circuits and Systems, Vol. 2, pp. 1-4, 2001.
24. W. L. Lee, Y. C. Chen and K. S. Hsieh, "Robust calculation of fractal dimension of images and its applications to classification of ultrasonic liver images and texture images," The 2002 IEEE International Symposium on Circuits and Systems, Vol. 2, pp. 656-659, 2002.
25. Wen-Li Lee, Yuan-Chang Chen and and Kai-Sheng Hsieh, " Ultrasonic Liver Tissues Classification by Fractal Feature Vector based on M-band Wavelet Transform, " IEEE Trans. Medical Imaging, vol. 22, no.3, pp. 382-392, March 2003.
26. B. B. Mandelbrot, Fractal Geometry of Nature. Freeman Press, San Francisco, 1982.
27. C. C. Chen, J. S. Daponte and M. D. Fox, "Fractal feature analysis and classification in medical imaging," IEEE Trans. Medical Imaging, vol. 6, pp. 133-142, June 1989.
28. S. C. Liu and S. Chang, "Dimension estimation of discrete-time fractional Brownian motion with applications to image texture classification," IEEE Trans. Image Processing, vol. 6, no. 8, Aug. 1997.
29. N. Sarkar and B. B. Chaudhuri, "An efficient differential box-counting approach to compute fractal dimension of image," IEEE Trans. Systems

Man and Cybernetics, vol. 24, pp. 115-120, Jan. 1994.
30. S. Buczkowski, S. Kyriacos, F. Nekka, and L. Cartilier, "The Modified Box-Counting Method: Analysis of Some Characteristic parameters," Pattern Recognition, vol. 31, No. 4, pp. 411-418, 1998.
31. J.M. Keller, S. Chen, and R.M. Crowniver, "Texture description and segmentation through fractal geometry," CVGIP, 45, pp.150-166, 1989.
32. J. Feng, W-C Lin, and C-T Chen, "Fractional box counting approach to fractal dimension estimation," Proceedings, 13th ICPR, vol II, pp.854-858, 1996.
33. S. Chen, J.M. Keller, and R.M. Crowniver, "On the calculation of fractal features from images," IEEE Trans. Pattern Anal. and Machine Intell., vol. 15, no. 10, pp. 1087-1090, Oct. 1993.
34. Campbell, F.W. and Robson, J.G., "Application of Fourier Analysis to the Visibility of Gratings," J. Physilogy, vol.197, pp.551-566, 1968.
35. De Valois, R.L. Albrecht D.G., and Thorell, L.G., "Spatial-Frequency Selectivity of Cells in Macaque Visual Cortex," Vision Research, vol.22, pp.545-559, 1982.
36. S. Mallat, "A theory for multiresolution signal decomposition: the wavelet representation," IEEE Trans. Pattern Anal. and Machine Intell., vol. 11, pp. 674-693, July 1989.
37. O. Rioul and M. Vetterli, "Wavelets and signal processing," IEEE Signal Processing Mag., vol. 8, no. 4, pp. 11-38, Oct. 1991.
38. G. Strang and T. Nguyen, Wavelets and Filter Banks. MA: Wellesley-Cambridge, 1996.
39. P. P. Vaidaynathan, Multirate Systems and Filter Banks. New Jersey: Prentice-Hall, 1993.
40. C. S. Burrus, R. A. Goponath, and H. Guo, Introduction to wavelets and wavelet transform: a primer. New Jersey: Prentice-Hall, 1998.
41. I.Daubechies, "The wavelet transform, time-frequency localization and signal analysis," IEEE Trans. Information Theory, vol. 36, pp.961-1005, Sept. 1990.
42. R. A. Goponath, E. Odegard, and C. S. Burrus, "Optimal wavelet representation of signals and the wavelet sampling theorem," IEEE Trans. Circuits and systems. II, vol. 41, no. 4, pp. 262-277, April 1994.
43. M. K. Tsatsanis and G. B. Giannakis, "Principal Component Filter Banks for Optimal Multiresolution Analysis," IEEE Trans. Signal Processing, vol. 43, No. 8, pp. 1766-1777, Aug. 1995.
44. P. Steffen, P. N. Heller, R. A. Goponath, and C. S. Burrus, "Theory of Regular M-Band Wavelet Bases," IEEE Trans. Signal Processing, vol. 41, No. 12, pp. 3497-3511, Dec. 1993.
45. Y. Chitre and A. P. Dhawan, "M-band wavelet discrimination of nature textures," Pattern Recognition, vol. 32, pp. 773-789, 1999.
46. R. O. Duda and P. E. Hart, Pattern Classification and Scene Analysis. New York: Wiley, 1973.
47. M. Nadler and E. P. Smith, Pattern Recognition Engineering. New York: Wiley, 1993
48. K. Fukunaga, Introduction to Statistical Pattern Recognition. Academic Press, San Diego, 1990.
49. M. T. Hagan, H. B. Demuth, and M.H. Beale, Neural Network Design, Boston, MA: PWS Publishing, 1996.
50. D. F. Specht, "Probabilistic neural network," Neural Networks, vol. 3, no. 1, pp. 109-118, Jan. 1990.
51. D. F. Specht, "Probabilistic neural network and the polynomial adaline as complementary techniques for classification," IEEE Trans. Neural Networks, vol. 1, no. 1, pp. 111-121, Mar. 1990.
52. P. Burrascano, "Learning vector quantization for the probabilistic neural network," IEEE Trans. Neural Networks, vol. 2, pp. 458-461, 1991.
53. E-Liang Chen, Pau-Choo Chung, Ching-Liang Chen, Hong-Ming Tsai, and Chein-I Chang, "An automatic diagnostic system for CT liver image classification," IEEE Trans. Biomedical Engineering, vol. 45, no. 6, June 1998.
54. P. J. Scheuer, "Pathologic types of hepatic tumors," in Liver cell carcinoma, P. Bannasch, D. Keppler, and G. Weber, Eds. New York: Kluwer-Academic, p.18, 1989.
55. J. H. Lefkowitch, "Pathologic diagnosis of liver disease," in Hepatology: a Textbook of liver Disease, D. Zakim and T. D. Boyer, W. B. Saunders, Eds. London, England, p.719, 1990.